PHOTOSTABILITY OF β-CAROTENE/MODIFIED KAOLINITE

Nelly Wahyuni[1,4] Georges Zissis[2] Zéphirin Mouloungui[1,3]*

[1]Université de Toulouse, INP-ENSIACET, LCA (Laboratoire de Chimie Agro-industrielle), 4 Allée Monso, F-31030 Toulouse, France

[2] Université de Toulouse, Université de Toulouse, LAPLACE (Laboratoire Plasma et Conversion d'Energie), UPS, INPT, 118 route de Narbonne, F-31062 Toulouse, France

[3] INRA, UMR 1010 CAI, F-31030, Toulouse, France

[4]Department of Chemistry, Mathematics and Natural Sciences, Tanjungpura University, Jl. Prof. H. Hadari Nawawi, Pontianak 78124, Indonesia

*zephirin.mouloungui@ensiacet.fr

Abstract: β-carotene (BC), a natural organic compound, is very highly sensitive to light. The stability of BC can be improved by various methods. The aim of this study was to propose a simple method for improving the photostability of BC with modified kaolinite (MK). MK was produced by kaolin modification, through calcination and interaction with $ZnCl_2$. The characteristics of the MK were determined by using scanning electron microscope–energy dispersive X-ray spectroscopy (SEM-EDX), X-ray diffraction (XRD), infrared spectroscopy (IR), and surface area analyzer. The photostability of BC was measured with a UV-spectrophotometer. The XRD patterns of the kaolinite showed layer disruption during calcination at 600°C, leading to metakaolinite production. Surface area analysis and IR-spectroscopy revealed an increase in mean pore volume in the MK and a shift of the signal for the –OH group, respectively. MK decreased the photodegradation of BC, and increased

the half-life of this molecule by almost 15-fold than the only BC 1.44 h. The amount of BC photostabilized by MK expressed as percentage of photostability, at five hours it was 61.87%. The amount of BC adsorbed onto the kaolinite was related to the photostability of BC.

Key-words: β-carotene, half-life, kaolin, metakaolinite, modified kaolinite, photodegradation, photostability

INTRODUCTION

The demand for β-carotene (BC) is increasing, as this molecule can serve as a precursor of vitamin A, anticancer agent, nutraceutical, food colorant, in photoprotectant and cosmetic preparations, and for the prevention of age-related molecular degeneration (Palozza *et al*., 2004; Van Keulen *et al*., 2010; Wong *et al*., 2011; Freitas *et al*., 2015). These multiple uses are related to the antioxidant properties of carotenoids, which have a conjugated polyene structure that is highly effective for free radical and singlet oxygen scavenging (Siems *et al*., 2005; Mueller and Boehm, 2011). Natural BC can be extracted from carrot (Suryana *et al*., 2013) or produced by biotechnological processes involving the use of filamentous fungi, yeasts, bacteria or microalgae (Thakur and Azmi, 2013). More than 85% the BC available on the market is now produced through chemical synthesis (Van Keulen *et al*., 2010). BC absorbs light at wavelengths of 415 to 508 nm. It could, therefore, potentially be used as a sensitizer in the dye sensitizer solar cell (DSSC) (Suryana *et al*., 2013).

The long chain of alternating double bonds (conjugated) of BC is responsible for its color. The axis of the carbon chain is curved, but the conjugated double bonds play an important role in ensuring that the molecule remains, stable, and rigid. Furthermore, the π-

electrons in the chain are also delocalized, loosely held in place, and easily excited by low-energy visible light.

Baro and his colleagues studied the self-organisation of layers of BC molecules on the surface of Cu_{111} and reported that BC was a good electron transfer molecule. Within the multilayer structure, electrons flow easily from molecule to molecule within layers and to the layer below, due to the attractive interaction connecting the π-electron orbitals of adjacent molecules. They also reported the total length of the molecule to be 3.8 nm, with a height of 0.5 nm. A schematic molecular model of BC is shown in Figure 1.

BC is sensitive to the light, temperature, and oxygen, and the mechanisms by which it is degraded have been investigated in many studies. The thermal degradation of BC is responsible for the color change observed in pumpkin puree (Dutta *et al*., 2006). Visible changes in color have been shown to be a direct manifestation of changes in BC content.

Following the absorption of ultraviolet (UV) light, organic compounds move from the ground state to singlet excited states, in which molecules may undergo intersystem crossing (ISC) to reach the triplet excited state or internal conversion (IC) back to the ground state. Thus, in terms of photostability, molecules displaying high rates of IC are the most desirable (Osterwalder and Herzog, 2009). Free radicals and photoproducts are generated by photochemical reactions in both the singlet and triplet excited states (Freitas *et al*., 2015). In previous studies, most of the photocatalytic products of BC were identified in other systems, such as the thermal degradation of BC. Esters, ketones, alcohols, and aldehydes are the principal degradation products of the photocatalytic degradation of BC (Ge *et al*., 2015).

Some studies have focused on improving pigment stability. For example, the stability of curcumin was found to be increased by complexation with divalent ions such as Zn^{2+} (Zebib *et al*., 2010). The encapsulation of BC has been shown to improve its stability and facilitate the effective delivery of this molecule in various food systems and applications (Gul *et al*., 2015). The photostability of the natural pigment can be enhanced by the use of a photoprotector, such as gold nanoparticles (AuNPs), as demonstrated for chlorophyll-*a* (Chla). AuNPs bind to the nitrogen site of Chla, thereby preventing the binding of reactive oxygen species to this site, which is known to cause the photodegradation of Chla. The ability of AuNPs to protect Chla effectively, and not just through antioxidant properties, opens up new possibilities for increasing the photostability of other types of porphyrins. These molecules are widely used for industrial (in optoelectronic devices, such as organic light emitting diodes (OLEDs) and photovoltaic devices) and medical (photodynamic therapy) applications (Barazzouk *et al*., 2012). The immobilization of bixin on activated kaolinite increased the photostability of pigment and this matrix has been used in DSSCs (Hiendro *et al*., 2012; Rahmalia, 2016).The complexation of BC with humic acid (hypothetically, a π–π interaction) affects its chemical properties, increasing its photostability and water solubility (Martini *et al*., 2010).

Minerals, such as quartz, and kaolin clay are abundant in West Kalimantan, Indonesia (Destiarti *et al*., 2017). Kaolin is widely used for processes requiring clays in industry. The applications for which it is suitable depend on its surface reactivity. Kaolin is most frequently used as a filler in polymers, rubber, paper, cosmetics, and medicines (Zsirka *et al*., 2015). However, it can also be used as an adsorbent, catalyst, composite, nanohybrid, and electrode

coating (Tonlé *et al*., 2011; Matusik *et al*., 2011; Araujo *et al*., 2014; Dedzo and Detellier, 2014; Matusik and Matykowska, 2014), provided that the surface and its structure are modified.

The properties of kaolinite can be improved by two principal treatments: (a) physical modification, and (b) chemical treatment with acids, bases, or organic compounds. Heating or microwave treatment can be used to induce physical modifications due to changes in chemical composition and crystalline structure at high temperature. Acids, bases, or organic compounds can be used for chemical modification, usually through changes to structure, surface functional groups, and surface area (Kumar *et al*., 2013).

Thermal and chemical treatments have been used to improve the properties of kaolinite. Calcination, at type of thermal treatment, generates metakaolinite, which is more reactive than the original substance. Kaolin from Navalacruz, Zamora province, west of Spain has a Brunauer-Emmett-Teller (BET) surface area of 18 m^2/g. The calcination of this kaolin at 600°C followed by activation with HCl yields a material with a specific surface area of 219 m^2/g (Belver *et al*., 2002). Other reported activation conditions have involved the use of H_2SO_4 (Hattab *et al*., 2013), CH_3COOH, H_3PO_4, HCl, HNO_3, and NaOH (Kumar *et al*., 2013). Metakaolinite has been activated by H_3PO_4, to increase dielectric performance by reducing dielectric permittivity and electrical conductivity, making this geopolymers suitable for use as encapsulating materials (Douiri *et al*., 2016).

Kaolin and metakaolin have been used as cheap adsorbents for the removal of metal ions, such as Cd^{2+}, Cu^{2+}, Pb^{2+}, and Zn^{2+} (Srivastava *et al*., 2005; Mbaye *et al*., 2014; Chai *et al*., 2017). The conversion of kaolin into metakaolin increases its ability to adsorb metal ions,

by increasing its surface area, pore volume or ability to take up water (Esomba *et al*., 2014).

Dyes molecules are stabilized by inorganic host materials due to the solid acidity and shielding effect from external circumtances by incorporation into the *nano-space* of clay, zeolit or mesoporous (Kohno *et al.*, 2011). The introduction of Al^{3+} and Fe^{3+} to mesoporous silicas forms acid sites, resulting in the sufficient stabilization of the flavylium. Since the stability enhancement of the BC using mesopores silica due to the inclusion of this molecule deep inside the mesopore contributed to the stabilization and tight fixation of this molecule (Kohno *et al*., 2016), the stabilization of the this dye can be expected through the incorporation into the Zn-modified kaolinite.

The objectives of this research were to study the photostability and degradation kinietic of BC with modified kaolinite (MK) under UV irradiation. Metakaolinite-Zn is expected increase the interaction of BC with MK, which correlate to the amount of BC absorbed. The unabsorbed BC related to the stability of this natural dye.

MATERIALS AND METHODS

The raw kaolin used came from Capkala region, West Kalimantan province, Indonesia. Separation was performed by aqueous decantation (3 times) and centrifugation at 6000 rpm for 10 min for enrichment of the clay fraction. The chemical composition of this fraction was follows: 51.82% SiO_2, 43.91% Al_2O_3, 1.19% MgO, 0.91% TiO_2, 0.87% Fe_2O_3, 0.10% CaO, and loss by ignition. According to the BET theory, the specific surface area of kaolin (K) was 35.414 m^2/g. BC (purity > 97%) used is a United Stated Pharmacopeia (USP) reference standard. The chemical reagents were analytical grade with purity more than 98% for $ZnCl_2$ and acetone > 99.5%. The chemical reagents and BC were obtained from Sigma

This is a 'pre-publication' version of an accepted article for Clays and Clay Minerals.
This version may be subject to change during the production process.
The DOI given, which may be used for citation purposes, though which will not be active until the version of record is published, is DOI: 10.1346/CCMN.2018.064115

Aldrich (Saint Louis, Missouri, USA). Kaolin (250 mesh) was calcined in a furnace at 600°C for 6 h to produce metakaolinite (MKaol) which was then modified by incubation with $ZnCl_2$. In total, 5 g MKaol was modified by interaction with 125 mL 0.08 M $ZnCl_2$ (pH = 6), with stirring, for 6 h. The mixture was decanted to separate out the solid fraction, which was dried (MK). BC (2.5 ppm in acetone) was interacted with the MK (BC/MK = 40 mL/1 g) for 1 h and then irradiated with UV light at 365 nm (flux = 1.6 W/m^2) for 9 h. The effluent was centrifuged for 5 min at 5000 rpm to separate the solid particle thus only liquid (BC) will be analyzed. Around 3 mL of the effluent were mesured with UV-VIS spectrophotometer. The absorption spectra of BC were identified until 9 h of UV irradiation. BC concentration before and after irradiation were determined with a standard curve equation : $y = 0.279x + 0.167$ (x = BC concentration (ppm), y = absorbance, and the correlation coefficient, $R^2 = 0.997$).

The raw kaolin was characterized by scanning electron microscopy- energy dispersive X-ray spectroscopy (SEM-EDX), X-ray diffraction (XRD), infrared spectroscopy (IR), and nitrogen adsorption. Micrographs were obtained with SEM model JSM 7100 F, manufactured by Jeol, Origon, USA, at an accelerating voltage of 10 kV. The samples were deposited on a sample holder with adhesive carbon foil and sputtered with gold. The mineral phases were investigated with XRD instrumentation by Bruker AXS GmbH (Billerica, Massachussets, USA) using Ni filtered CuKα radiation (λ = 0.154 nm) in Bragg-Bretano geometry with a scanning rate of 10°/min from 4° to 80° (2θ). The patterns obtained were analysed with Bruker-D8 software. The IR spectra were recorded for the 4000-400 cm^{-1} region, with a Perkin-Elmer SHIMADZU IR spectrometer and the KBr pellet technique. The apparatus used was fabricated by SHIMADZU at Kyoto, Japan. Textural analyses were performed on the

corresponding nitrogen adsorption-desorption isotherms at 77 K (BET method). The nitrogen adsorption isotherms were obtained from BELSORP-max manufacturer by BEL JAPAN Inc, Osaka, Japan. Nitrogen adsorption data were obtained with about 0.2 g of sample. The samples were degassed for one hour at 90°C, with heating at a rate of 4°C/min. BET equations were applied to the isotherms to determine the specific surface area. The absorption spectrum of BC was obtained with a UV-1800, UV-VIS spectrophotometer by Shimadzu Scientific Instrumentation Inc, Kyoto, Japan.

Photodegradation and life-time of BC calculated by determining the reaction rate constant by Santoso *et al*. (2007), modified from first-order rate equation from Lagergren's. Lagergren's first-order rate equation has been called pseudo-first-order to distinguish kenetic equation of liquid-solid phase adsorption base on adsorption capacity from concentration of solution (Qiu *et al*., 2009; Sejie *et al*., 2016). The change in the absorption at λ_{max} under visible light irradiation was expressed by the time dependence of the ratio A/A_0 (A=absorption at time t, A_0=absorption at time t=0). Plot of ln % absorbance (A/A_0) to the irradiation time resulted a straight line can be obtained, where the slope is k, and $t_{1/2}$ is calculated.

The percentage photostability of BC in the presence of the MK was then calculated as previously described (Claes, 1960), with the following formula:

$$\frac{E_3 - E_2}{E_1 - E_2} \times 100 \qquad (1)$$

where E_1, E_2, and E_3 are the concentrations (or absorbances) of BC before irradiation, after irradiation without MK, and after irradiation in the presence of MK, respectively.

RESULTS

The kaolin from West Kalimantan, Indonesia (Figure 2) used here had a reasonably homogeneous morphology. It consisted of small platelets of different sizes, pseudohexagonal or hexagonal in shape, as typically observed for kaolinite (Sengupta *et al*., 2008). The characteristic randomly oriented platelets of kaolinite were stacked to form large grains of a few micrometres in size (Figure 2b) (Araujo *et al*., 2014).

The XRD patterns of K, MKaol, and MK are shown in Figure 3. The raw kaolin consisted of kaolinite associated with quartz and a small muscovite fraction. The reflections observed at 7.15, 3.57, and 2.3 Å indicated the presence of a second phase, identified as kaolinite. The 001 basal distance of kaolinite is 7.2 Å (Zsirka *et al*., 2015). Calcination at 600°C for 6 h gave 001 and 002 basal reflections of destroyed kaolinite, indicating a collapse of the structure of the material and production of MKaol through dehydroxylation. MKaol is an unstable phase of kaolinite, and its production can be represented as a simple equation (Ilić *et al*., 2010).

$$Al_2O_3{\cdot}2SiO_2{\cdot}2H_2O \rightarrow Al_2O_3{\cdot}2SiO_2 + 2H_2O\uparrow \qquad (2)$$

The modification of MK with $ZnCl_2$ had no significant effect on the XRD pattern. Md Saad *et al*. (2016) found that copper ions were adsorbed onto kaolinite with no change in structure.

On the IR spectrum of K (Figure 4), absorption peaks at 3697 cm^{-1}, 3653 cm^{-1}, and 3620 cm^{-1} were identified as corresponding to the stretching vibration of internal hydroxyl bonds (Al..O..H) in the octahedral sheet identified as kaolinite. The wavenumber at 3435 cm^{-1} corresponds to the stretching vibration for the –OH bond of H_2O, whereas a deformation of

this bond is observed at 1631 cm^{-1} (Sengupta *et al*., 2008). The bands at 1112 cm^{-1}, 1032 cm^{-1}, and 1000 cm^{-1} were assigned to Si-O stretching. Al-OH deformation bands were identified at 912 cm^{-1} and 753 cm^{-1}. Al-O-Si deformation was detected at 538 cm^{-1} and Si-O-Si deformation at 470 cm^{-1} (Belver *et al*., 2002; Hattab *et al*., 2013; Kumar *et al*., 2013; Vaculikova *et al*., 2011). The presence of quartz was confirmed by the doublet at about 800 and 775 cm^{-1} (Vizcayno *et al*., 2010).

Calcination converted the kaolinite into MKaol, as demonstrated by the disappearance of the band at 3697-3620 cm^{-1}, confirming the dehydroxylation of kaolinite. The presence of a band at 1631 cm^{-1}, corresponding to H_2O molecules on the MKaol reflects the hygroscopic nature of MKaol after heating at 600°C (Tchakouté *et al*., 2012). Furthermore, the transmittance intensity of the Al-O functional group decreased or the fingerprint bands disappeared on the spectra for MKaol and MK.

Assessments of the stability of BC without irradiation (Figure 5a) revealed a maximum peak for BC in acetone at 452 nm, with other peaks observed at 486 nm and 426 nm. The degree of the photodegradation is expressed as the change in the main absorption band of BC at 452 nm. The BC concentration was relatively unchanged after being stored for nine hours at room condition. Under irradiation, the absorbance of BC (Figure 5b) decreased significantly at 5 h, with absorbance reaching levels close to zero at 7 h. By contrast, the absorbance of BC/MK (Figure 5c) remained high for nine hours, even under irradiation. MK therefore increased the photostability of BC.

The rate constant of photodegradation BC declined by the present of MK (Figure 6b). Kinetic analyses of the photodegradation of BC and BC/MK showed the half-life of BC

in the presence of MK to be four times that in its absence (Table 1).The percentage photostability of 40 mL BC with 1 g MK (40 mL/1g) was 23.82%. Photostability increased to 52.76% and 61.87% for BC interacting with MKaol and MK, respectively. The percentage photostability reflects the amount of BC adsorbed onto the K, MKaol, or MK. The amount of BC absorbed onto K, MKaol, and MK were 1.46 ppm, 1.93 ppm, and 2.01 ppm. Therefore 58.34%, 77.31%, and 82.29% of the inisial concentration BC are photostabilized by the K, MKaol, and MK, respectively.

The percentage photoprotection was calculated using equation (1), as described in the experimental section.

The maximal percentage photostability of BC (Figure 7) was achieved with 1 g of MK. The photostability of BC decreased with decreases in the mass of MK. The percentage photostability of this matrix was 61.87%.

DISCUSSION

The permanent negative charge of kaolinite results from the isomorphic replacement of Si^{4+} in the silica tetrahedral sheet by Al^{3+} or the replacement of trivalent metal ions (such as Al^{3+}) by divalent ions (such as Fe^{2+} and Mg^{2+}) in the octahedral alumina sheet. Each substitution results in a single negative charge. Both the alumina sheet and the crystal edges have a pH-dependent variable charge caused by the protonation and deprotonation of surface hydroxyl (SOH) groups (Srivastava *et al.,* 2005). MKaol is an unstable phase of kaolinite producted through dehydroxylation (Ilić *et al*., 2010). Dehydroxylation implies a reorganization and diffusion of hydroxyl group in the layer (Shvarzman *et al*., 2003). MKaol is more reactive than K due to the structural disorder such as deformation of silica network or

existence of 4-coordinated aluminium, which is more reactive than 6-coordinated aluminium. The unstable MKaol, also still contains about 10% of the OH-groups initially present in the K. Therefore, it is favourable to a surface dissolution of treated kaolin in cationic solution (Konan *et al*., 2009).The surface of the MKaol thus has some types of binding sites capable of interacting with Zn^{2+}. Essomba *et al*. (2014) studied the adsorption of cadmium onto kaolinite. They concluded that a chemisorption reaction or an activated process predominated in the rate-controlling step of the cadmium system. They also reported that metakaolinite had a higher adsorption capacity than kaolinite, due to its greater surface area, pore volume and hygroscopy.

Chai *et al*. (2017) reported that pH affected the mole fraction of hydrolyzed Zn^{2+} species relative to the total soluble metal concentration at 25°C. The main species present at pH values below 7 is Zn^{2+}. Chai *et al.* also concluded that electronic attraction was the main mechanism of Zn^{2+} adsorption on kaolinite. Transition metals adsorb at permanent and variable charge sites. Sites with a permanent negative charge can undergo an exchange reaction with Zn^{2+} at high pH. At this present study, $ZnCl_2$ solution was allowed to interact with MKaol at pH= 6, therefore Zn^{2+} was probably adsorbed onto MKaol via a SOH group.

$$SOH = SO^- + H^+ \quad (2)$$

$$2SO^- + Zn^{2+} = Zn(SO)_2 + H^+ \quad (3)$$

The absorption of energy by a compound or photosensitizer triggers photochemical damage to the substance concerned. Many photochemical reactions are complex and may involve serial competition for reaction pathways in which oxygen plays a significant role. Indeed, the vast majority of photoreactions involves the consumption of molecular oxygen

and is photo-oxidative processes. The photodegradation of BC is known to be essentially photo-oxidative, and is brought about by various reactive oxygen species (ROS), such as singlet oxygen and superoxide (Barazzouk *et al*., 2012). The absorption of UV light by BC results in the formation of its excited singlet (^{1}BC*). Mordi proposed a mechanism for BC degradation in which BC is degraded by *cis-trans* isomerization, followed by the formation of a singlet diradical. The oxygen attack on either side of the *cis* bond is enhanced, through the generation of other types of radical species, and further reactions occur until the final product is produced (Mordi, 1992).

According to BET surface area analysis (Table 2), calcination decreased the specific surface area, but increased total pore volume and mean pore volume. The surface area of kaolin decreased from 18.2 m^2/g into10.6 m^2/g during calcination at 600° for 10 h (Belver *et al*., 2002). Essomba *et al*. (2014) reported that calcination kaolin at 700° for 6 h increased specific surface area and pore volume. The surface area to be 20 and 33 m^2/g, while pore volume from 0.0814 and 0.0935 cm^3/g, respectively. Therefore, the decreasing of surface area is consistent with Belver *et al*., but contradiction with Esomba *et al*., due to the chemical composition of natural kaolin was used. The major component was anatase associated with illite, quartz, kaolinite, and lepidocrocite (Esomba *et al*., 2014).

BC absorption occurred in meso-sized pores. This physical adsorption involved van der Waals forces. The higher adsorption capacity of MKaol than of K may be due to the presence of larger pores (Table 2). MKaol pore size was markedly larger than the cross-sectional dimensions of the monomeric BC molecule, consistent with the findings of Worasith *et al.* (2011), resulting in a large periodic multilayer (Baro *et al*., 2003). Srasra and

Trabelsi-Ayedi (2000) proposed the possiblity chemical interaction of BC with the surface of the clay (Figure 8). This mechanism involved the hydrogen bonding BC to Brönsted sites and/or direct binding at Lewis sites through the formation of carbonium ions or coordinating bonds (Sarier and Güler, 1988). The interaction also involved the breaking of bonds in the dissolved octahedral and tetrahedral sheets (Adams, 1987).

Zinc ions intercalate into MKaol by electronic attraction. The aggregation of MKaol particles results from the adsorption of positively charged Zn^{2+} ions onto the surfaces of this solid material (Chai *et al*., 2017). The presence of zinc ions in the MKaol increased the interaction of BC with this solid material. The analysis of EDX spectra showed that the MK contained 6.1%. According to Zebib *et al*. (2010), who described a hypothetical mechanism of Zn^{2+} intercalation with curcumin and the structural model of BC (Srasra and Trabelsi-Ayedi, 2000), interaction between MK and BC may modify complexation, with zinc as a Lewis site and BC as the electron donor. This mechanism increases the adsorption capacity of BC on MK. Acid site contributed to the stabilization of dye on mesoporous material (Kohno *et al.*, 2011). No distinction was made between aluminol and silanol surface groups, but the SOH groups involved in adsorption were probably mostly those of aluminol and AlOH (Schindler *et al*., 1987).

$$Zn(SO)_2 + 2\beta\text{-carotene} \rightarrow (SO)_2Zn \ldots 2\beta\text{-carotene} \qquad (4)$$

The absorbance of BC/MK decreased after irradiation, but the λ_{max} was almost unchange. This fact indicating there was only a simple degradation, but not photochemical conversion such as isomerization (Henry *et al*., 1998; Kohno *et al*., 2009; Xiao *et al*., 2018). It has been reported that the stability of BC related to order molecular association (Baro *et al*.,

2003). As the spectral shift was not observed, only a little changing in shape spectral, it was suggested that BC formed aggregation with the disorder orientation. Aggregation also contributed to the stability improvement of dye, because the aggregation reduced the contact area to the oxygen (Kohno *et al*., 2015).

The MK protected BC from the effects of direct UV irradiation. Lower levels of triplet oxygen and ROS formation were observed in the presence of MK. Carotenoid degradation was a direct result of irradiation. The shielding effect of the inorganic host material reduced the rate of degradation and also protected BC against ROS (Kohno *et al*., 2016).

Increasing the mass of MK to 2 g (Figure 7) decreased the percentage photostability of BC significantly, due to a decrease in capacity of BC to adsorb onto the MK. Overlaps between adsorption sites or their aggregation as a result of overcrowding decreased the adsorption capacity of BC (Essomba *et al*., 2014; Ndongo Kounou *et al*., 2015). The lower level of adsorption at higher mass also reflects the increase in interactions between the particles of a material with mass. The excess of amount of cation caused the precipitation of dye aggregate (Kohno *et al*, 2015). Therefore, BC photostability decreased with increasing the mass of MK also due to excessive amounts of Zn^{2+}.

However, this finding is not consistent with the results of Barazzouk and coworkers, who reported that the protection against Chla photodegradation afforded by AuNPs eventually reached a plateau (Barazzouk *et al*., 2012), this phenomenon being correlated to photoprotector particle size. When MK, which has micrometre-range particles, was used as photoprotector, the interactions between particles increased with mass. In the presence of

excess MK, the interaction of BC with MK decreased, and the BC was irradiated with UV light.

No significant difference was observed between the infrared spectra of MK and BC/MK (not shown).

CONCLUSIONS

SEM, XRD, and IR analysis showed that raw kaolin from West Kalimantan, Indonesia consisted of kaolinite associated with quartz and a small fraction of muscovite. The conversion of kaolinite to MKaol by calcination and the modification of MKaol with Zn^{2+} decreased the photodegradation of BC by shielding and protecting it against direct UV irradiation, leading to a 15-fold increase in half-life. The mass of MK influenced the photostability of BC. The percentage photostability of BC with MK at 5 h was 61.87% (40 mL BC/g MK). Photostability was related to the amount of BC adsorbed onto the kaolinite. The use of MK as a photostabiliser of BC is a new method in which MKaol-zinc can be used. This method could also be applied to other metal ions and pigments. This composite material has potential applications in cosmetics (sunscreen) or in photovoltaics (DSSCs).

ACKNOWLEDGMENT

This study was financially supported by the Directorate General of Higher Education, Ministry of Research, Technology and Higher Education of Indonesia.

References

Adams, J.M. (1987) Synthetic organic chemistry using pillared, cation-exchanged and acid-treated montmorillonite catalysts – A review. *Applied Clay Science*, **2**, 309 – 342.

Araujo, F.R., Baptitta, J.G., Marcal, L., Ciuffia, K.J., Nassara, E.J., Calefi, P.S., Vivcente,

M.A., Trujilano, R., Rives, V., Gilc, A., Korilic, S., and De Faria, E.H. (2014) Versatile heterogeneous dipicolinate complexes grafted into kaolinite: Catalytic oxidation of hydrocarbons and degradation of dyes. *Catalysis Today*, **227**, 105-115.

Baro, A.M., Hla, S., and Rieder, K.H. (2003) LT-STM study of self-organization of β-carotene molecular layers on Cu (1 1 1). *Chemical Physics Letters*, **369**, 240–247.

Barazzouk, S., Bekalé, L., and Hotchandani, S. (2012) Enhanced photostability of chlorophyll-*a* using gold nanoparticles as an efficient photoprotector. *Journal Materials Chemistry*, **22**, 25316-25324.

Belver, C., Banares, M.A., and Vicente, M.A. (2002) Chemical activation of a kaolinite under acid and alkaline conditions. *Chemistry of Materials*, **14**, 2033-2043.

Chai, W., Huang, Y., Su, S., Han, G., Liu, J., and Yijun, C.Y. (2017) Adsorption behavior of Zn(II) onto natural mineral minerals in wastewater. A comparative study of bentonite and kaolinite. *Physicochemical Problems of Mineral Processing*, **53**, 264−278.

Claes, H. (1960) Interaction between chlorophylls and carotenes with different chromophoric groups. *Biochemical and Biophysical Research Communications*, **3**, 585-590.

Dedzo, G.K. and Detellier, C. (2014) Intercalation of two phenolic acids in an ionic liquid-kaolinite nanohybrid material and desorption studies. *Applied Clay Science*, **97-98**, 153-159.

Destiarti, L., Wahyuni, N., Prawatya, Y., and Sasri, R. (2017) Synthesis and characterization of mangan oxide coated sand from Capkala kaolin. *International Conference on Chemistry, Chemical Process and Engineering*, AIP Conference Proceeding **1823**, 020023 doi: 10.1063/1.4978096.

Douiri, H., Louati, S., Baklouti, S., Arous, M., and Fakhfakh, Z. (2016) Enhanced dielectric performance of metakaolin–H_3PO_4 geopolymers. *Materials Letters*, **164**, 299–302.

Dutta, D., Dutta, A., Raychaudhuri, U., and Chakraborty, R. (2006) Rheological characteristics and thermal degradation kinetics of beta-carotene in pumpkin puree. *Journal of Food Engineering*, **76**, 538–546.

Essomba, J.S., Ndi Nsami, J., Belibi Belibi, P.D., Tagne, G.M., and Ketcha Mbadcam, J. (2014) Adsorption of cadmium (II) ions from aqueous solution onto kaolinite and metakaolinite. *Pure and Applied Chemical Sciences*, **2**, 11-30.

Freitas, J.V., Lopes, N.P., and Gaspar, N.L. (2015) Photostability evaluation of five UV-filters, trans-resveratrol and beta-carotene in sunscreen. *European Journal of Pharmaceutical Science*, **78**, 79-89.

Ge, W., Chen, Y., Wang, L., and Zhang, R. (2015) Photocatalytic degradation of β-carotene with TiO_2 and transition metal ions doped TiO_2 under visible light irradiation. *Universal Journal of Chemistry*, **3**, 104-111.

Gul, K., Tak, A., Singh,A.K., Singh, P., Yousuf, B., and Wani, A.A. (2015) Chemistry, encapsulation, and health benefits of β-carotene - A review. *Cogent Food & Agriculture*, **1,** 1018696.

Hattab, A., Bagane, M., and Chlendi, M. (2013) Characterization of Tataouinen's raw and activated clay. *Chemical Engineering & Process Technology*, **4**, 1-5.

Henry, L.K., Catigani, G.L., and Schwartz, S.J. (1998) Oxidative degradation kinetic of lycopne, lutein, and 9-cis and all-trans β-carotene. *Journal of the American Oil Chemists Society*, **7**, 823-829.

Hiendro, A., Hadary, F., Rahmalia, W., and Wahyuni, N. (2012) Enhanced performance of bixin sensitized solar cells with activated kaolinite. *International Journal of Engineering Research and Innovation*, **4**, 40-44.

Ilić, B.R., Mitrović, A.A., and Miličić, L.R. (2010) Thermal treatment of kaolin clay to obtain metakaolin. *Hemijska industrija*, **64**, 351–356.

Kohno,Y., Kinoshita, R., Ikoma, S., Yoda, K., Shibata, M., Matsushima, R.,Tomita, Y., Maeda, Y., and Kobayashi, K. (2009) Stabilization of natural anthocyanin by intercalation into montmorillonite. *Applied Clay Science*, **42**, 519-523.

Kohno, Y., Senga, M., Shibata, M., Yoda, K., Matsushima, R., Tomita, Y., Maeda, Y., and Kobayashi, K. (2011) Stabilization of flavylium dye by incorporation into Fe-containing mesoporous silicate. *Microporous and Mesoporous Materials*, **141**, 77-80.

Kohno, Y., Kato, Y., Shibata, M., Fukuhara, C., Maeda, Y., Tomita, Y., and Kobayashi, K. (2015) Enhanced stability of natural anthocyanin incorporated in Fe-containing mesoporous silica. *Microporous and Mesoporous Materials*, **203**, 232-237.

Kohno, Y., Kato, Y., Shibata, M., Fukuhara, C., Maeda, Y., Tomita, Y., and Kobayashi, K. (2016) Fixation and stability enhancement of beta-carotene by organo-modified mesoporous silica. *Microporous and Mesoporous Materials*, **220**, 1-6.

Konan, K.L., Peyratout, C., Smith, A., Bonnet, J.-P., Rossignol, S., and Oyetola, S. (2009) Comparison of surface properties between kaolin and metakaolin in concentrated lime solutions. *Journal of Colloid and Interface Science*, **339**, 103-109.

Kumar, S., Panda, A. K., and Singh, R. K. (2013) Preparation and characterization of acid

and alkali treated kaolin clay. *Bulletin of Chemical Reaction Engineering & Catalysis*, **8**, 61-69.

Martini, S., D'Addario, C., Bonechi, C., Leone G., Tognazzi, A., Consumi, M., Magnani, A., and Rossi, C. (2010) Increasing photostability and water-solubility of carotenoids: Synthesis and characterization of β-carotene–humic acid complexes. *Journal of Photochemistry and Photobiology B: Biology*, **101**, 355–361.

Matusik, J., Stodak E., and Baranowski, K. (2011) Synthesis of polylactide/clay composites using structurally different kaolinites and kaolinite nanotubes. *Applied Clay Sciences*, **51**, 102-109.

Matusik, J. and Matykowska, L. (2014) Behavior of kaolinite intercalation compounds with selected ammonium salts in aqueous chromate and arsenate solutions. *Journal of Molecular Structure*, **1071**, 52-59.

Mbaye, A., Diop, M.A.K., Miehe-Brendle, C.A.K., Senocq, J., Maury, F., and Francis. (2014) Characterization of natural and chemically modified kaolinite from Mako (Senegal) to remove lead from aqueous solutions. *Clay Minerals*, **49**, 527-539.

Md Saad, N.S.S., Nik Malek, N.A.N., and Chong, C.S. (2016) Antimicrobial activity of copper kaolinite and surfactant modified copper kaolinite against gram positive and gram negative bacteria. *Sciences & Engineering*, **78**, 127–132.

Mordi, R.C. (1992) Mechanism of β-carotene degradation. *Biochemical Journal Letter* , 310.

Mueller, L. and Boehm, V. (2011) Antioxidant activity of β-carotene compounds in different *in vitro* assays. *Molecules*, **16**, 1055-1069.

Ndongo Kounou, G., Ndi Nsami, J., Belibi Belibi, D.P., Kouotou, D., Tagne, G.M., Dina Joh, D.D., and Ketcha Mbadcam, J. (2015) Adsorption of zinc (II) ions from aqueous solution onto kaolinite and metakaolinite. *Der Pharma Chemica*, **7**, 51-58.

Osterwalder, U. and Herzog, B. (2009) Chemistry and properties of organic and inorganic uv filters. Pp. 11-38 in: *Clinical Guide to Sunscreens and Photoprotection* (H.W. Lim and Z.D. Draelos, editors). Informa Healthcare, New York.

Palozza P., Serini, S., Nicuolo, F.D., and Calviello, G. (2004) Modulation of apoptotic signaling by carotenoids in cancer cells. *Archives of Biochemistry and Biophysics*, **430**, 104-109.

Qiu, H., LV, L., Pan, B-C., Zhang, Q-J ., Zhang, W-M, Zhang, Q-X. (2009) Critical review in adsorption kinetic models**.** *Journal of Zhejiang University SCIENCE A*, **10**, 716-724.

Rahmalia, W. (2016) Paramètres de performances de photo-électrodes de TiO_2/kaolinite et d'électrolyte a base de carbonates biosourcés dans la cellule solaire sensibilisée par la bixine. PhD Thesis, Institut National Polytechnique de Toulouse, Toulouse, France, 188 pp.

Santosa, S.J., Siswanta, D., Kurniawan, A., and Rahmanto, W.H. (2007) Hybrid of chitin and humic acid as high performance sorbent for Ni(II). *Surface Science*, **601**, 5155-5161.

Sarier, N. and Güler, C. (1988) B-carotene adsorption on acid activated montmorillonite. *Journal of American Oil Chemists Society*, **66**, 917–923.

Schindler, P.W., Liechti, P., and Westall, J.C. (1987) Adsorption of copper, cadmium and lead from aqueous solution to the kaolinite/water interface. *Netherlands Journal of Agricultural Science*, **35**, 219-330.

Sejie, F.P. and Nadiye-Tabbiruka, M.S. (2016) Removal of methyl orange (MO) from water by adsorption onto modified local clay (kaolinite). *Physical Chemistry*, **6**, 39-48.

Sengupta, P.C., Saiki, P.C., and Borthakur, P. (2008) SEM EDX characterization of an iron-rich kaolinite clay. *Journal of Scientific Industrial Research*, **67**, 812-818.

Shvarzman, A., Kovler, K., Grader, G.S., and Shter, G.E. (2003) The effect of dehydroxylation/amorphization degree on pozzolanic activity of kaolinite. *Cement and Concrete Research*, **33**, 405-416.

Siems, W., Wiswedel, I., Salerno, C., Crifo, C., Augustin, W., Schild, L., Langhans, C.D., and Sommerburg, O. (2005) β-carotene breakdown products may impair mitochondrial functions-potential side effects of high-dose β-carotene supplementation. *The Journal of Nutritional Biochemistry*, **16**, 385-397.

Srasra, E. and Trabelsi-Ayedi, M. (2000) Textural properties of acid activated glauconite, *Applied Clay Science*, **17**, 71–84.

Srivastava, P., Singh, B., and Angove, M. (2005) Competitive adsorption behavior of heavy metals on kaolinite. *Journal of Colloid and Interface Science*, **290**, 28–38.

Suryana, R., Khoiruddin., and Supriyanto, A. (2013) Beta-carotene dye of *Daucus carota* as sensitizer on dye-sensitized solar cell. *Material Science Forum*, **737**, 15-19.

Tchakoute K, H., Elimbi, A., Mbey, J.A., Ngally, S.C., and Njopwouo, D. (2012) The effect of adding alumina-oxide to metakaolin and volcanic ash on geopolymer products: A

comparative study. *Construction and Building Materials*, **35**, 960-969.

Thakur, M. and Azmi, W. (2013) Nutraceutical β-carotene from natural non-conventional sources and its applications. *Annals of Phytomedicine*, **2**, 59-73.

Tonlé, I.K., Letaif, S., Ngameni, E., Walcarius, A., and Detellier, C. (2011) Square wave voltammetric determination of lead (II) ions using a carbon paste electrode modified by a thiol-functionalized kaolinite. *Electroanalysis*, **23**, 245-252.

Vaculikova, L., Plevova, E., Vallova, S., and Kouttnik, I. (2011) Characterization and differentiation of kaolinites from selected Czech deposits using infrared spectroscopy and differential thermal analysis. *Acta Geodynamica et Geomaterialia*, **8**, 59–67.

Van Keulen, F., Carolas, A.L., Brito, M.L., and Ferreira, B.S. (2010) Production of high-purity carotenoids by fermenting selected bacterial strains. US Patent. 2010/0145116 A1.

Vizcayno, C., Gutierrez, R.M., Castello, R., Rodriguez, E., and Guerrero, C.E. (2010) Pozzolan obtained by chemical and thermal treatments of kaolin. *Applied Clay Science*, **49**, 405-413.

Wong, I.Y.H., Koo, S.C.Y., and Chan, C.W.N. (2011) Prevention of age related macular degeneration. *International Journal of Ophthalmology*, **31**, 73-82.

Worasith, N., Goodman, B.A., Jeyashoke, N., and Thiravetyan, P. (2011) Decolorization of rice bran oil using modified kaolin. *Journal of the American Oil Chemists' Society*, **88**, 2005-2014.

Xiao, Y-D., Huang, W-Y., Li, D-J., Song, J-F., Liu, C-Q., Wei, Q-Y., Zhang, M., and Yang, Q-M. (2018) Thermal degradation kinetics of all-trans and cis-carotenoids in a light-induced model system. *Food Chemistry*, **239**, 360-368.

Zebib B., Mouloungui Z., and Noirot V. (2010) Stabilization of curcumin by complexation with divalent cations in glycerol /water system. *Bioinorganic Chemistry and Applications*, 1-8.

Zsirka, B., Horvath, E., Mako, E., Kurdi, R., and Kristof, J. (2015) Preparation and characterization of kaolinite nanostructure: Reaction pathways, morphology and structural order. *Clay Minerals*, **50**, 329-340.

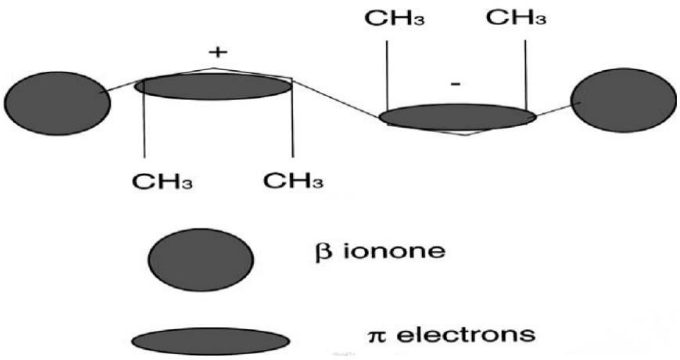

Figure 1. Schematic model of the β-carotene molecule, showing the curved backbone of the polyene chain, the methyl groups attached to it, the asymmetric corrugation attributed to π-electrons and the β-ionone rings (Baro *et al*., 2003)

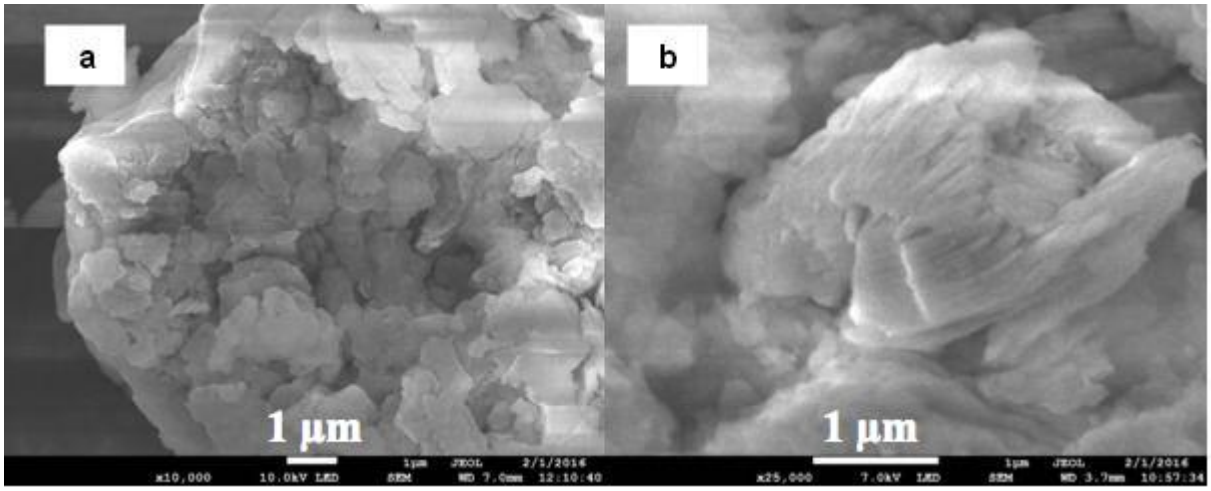

Figure 2. SEM micrographs of the kaolin from West Kalimantan, Indonesia at magnifications of (a) 10,000x and (b) 25,000x. Each of images showed a booklet morphology consisting of platelet sheet of kaolinite mineral with estimated average particle size about 2,0 µm.

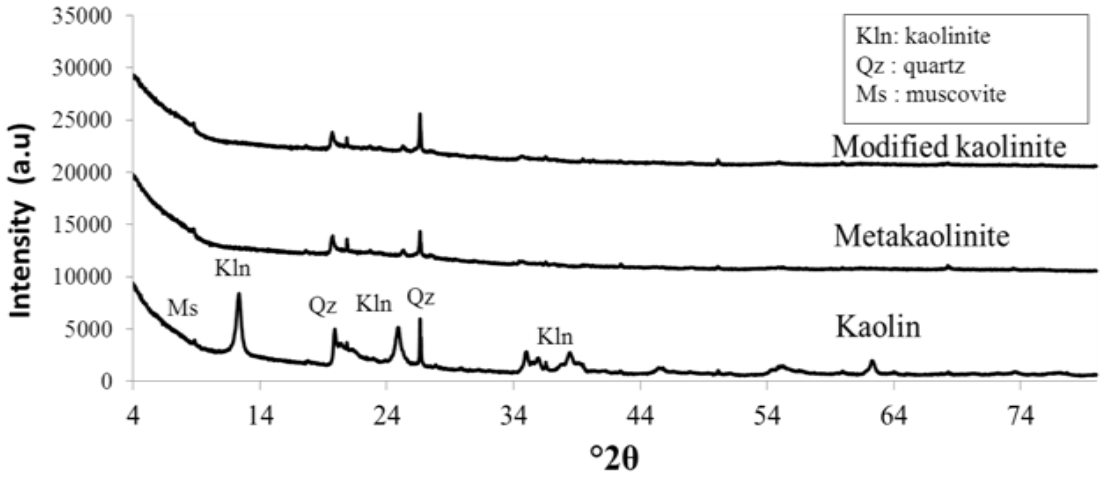

Figure 3. XRD pattern of kaolin, metakaolinite, and modified kaolinite

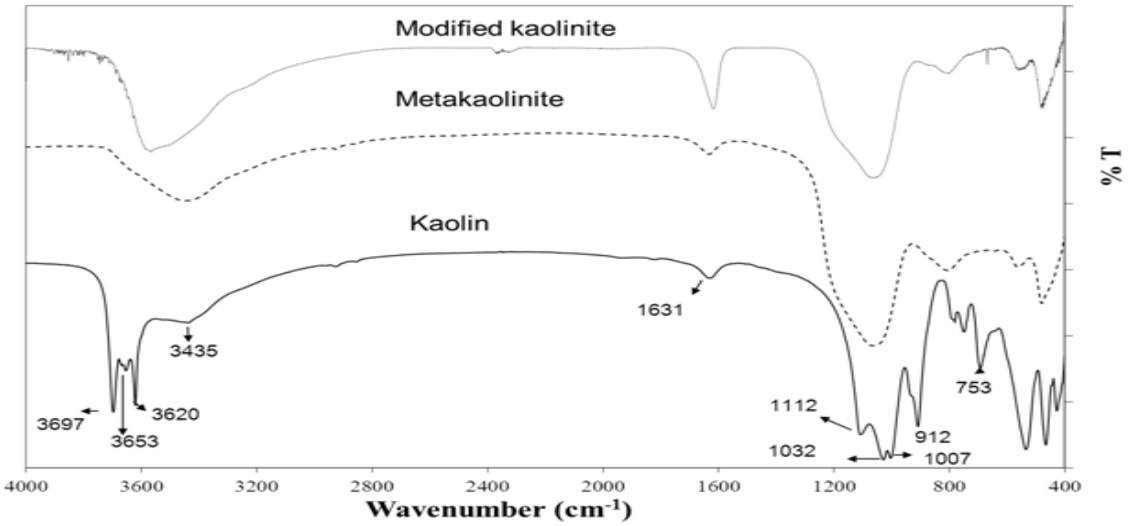

Figure 4. Infrared spectra of kaolin, metakaolinite, and modified kaolinite

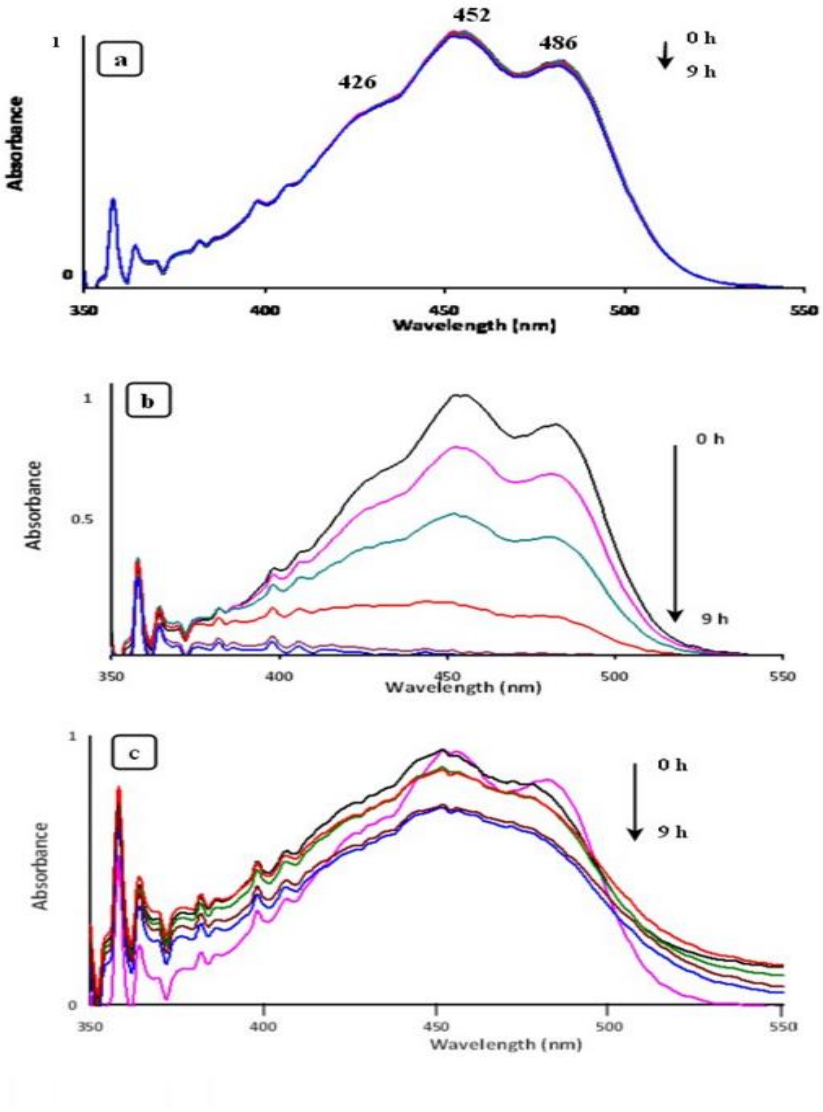

Figure 5. Absorption spectra of the products of (a) BC without irradition

(b) BC with UV irradiation, and (c) BC/MK under UV irradiation

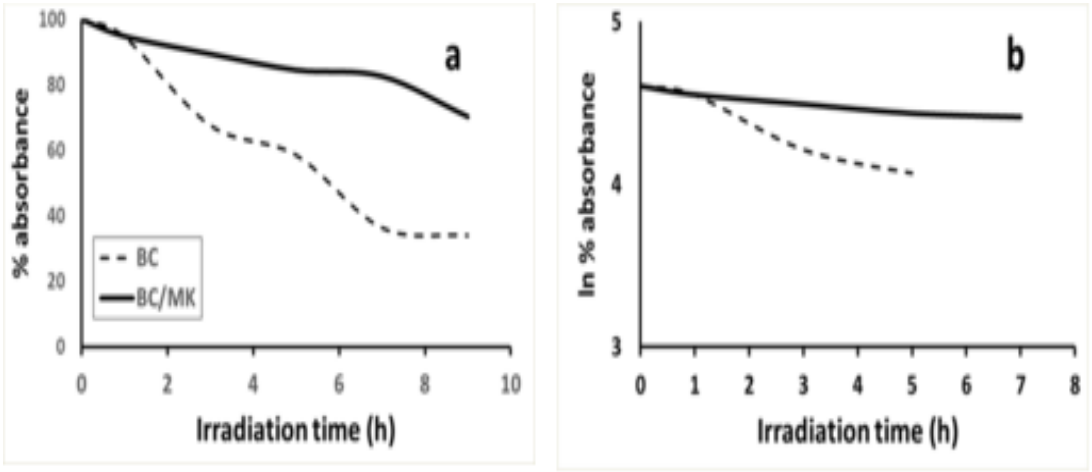

Figure 6. Kinetic photodegradation of β-carotene (BC) and β-carotene/modified kaolinite (BC/MK)

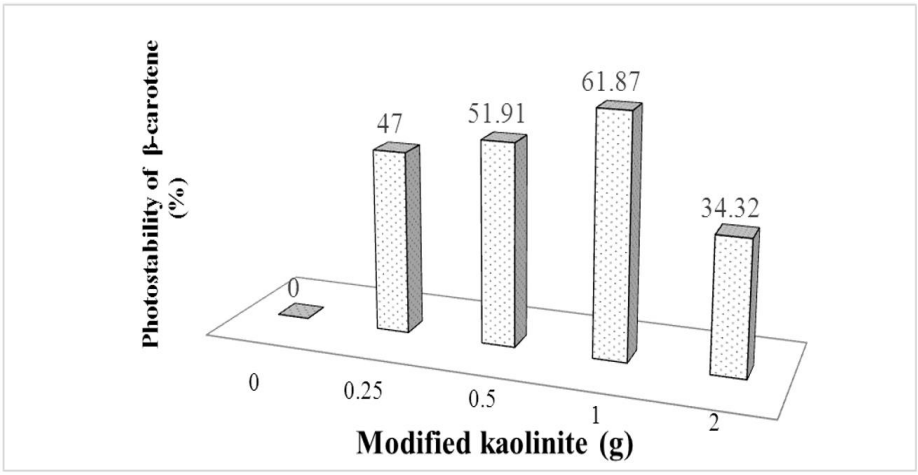

Figure 7. Photostability of β-carotene with different masses of modified kaolinite

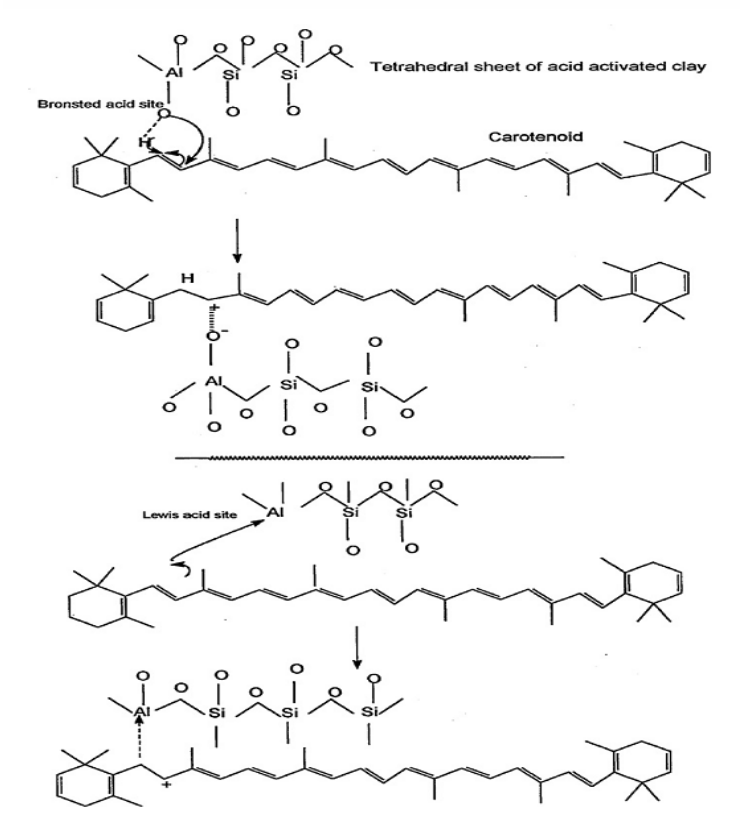

Figure 8. The mechanism of carotenoid adsorption on Brönsted and Lewis acid sites

(Srasra and Trabelsi-Ayedi, 2000)

Table 1. Pseudo-first-order reaction data for β-carotene (BC), β-carotene with kaolin (K), metakaolinite (MKaol), and modified kaolinite (MK)

Sample code	Correlation coefficient (R^2)	Rate constant, k (h^{-1})	Half-life, (h)	% Photostability at 5 h
BC	0.99	0.4854	1.43	-
BC/K	0.99	0.0833	8.32	23.82
BC/MKaol	0.96	0.0638	10.86	52.76
BC/MK	0.98	0.0325	21.32	61.87

Table 2. BET specific surface area, total pore volume, and mean pore size

Sample	Specific surface area (m^2/g)	Total pore volume (cm^3/g)	Mean pore volume (nm)
Kaolin	35.414	0.2006	22.660
Metakaolinite	23.193	0.2026	34.934
Modified kaolinite	23.805	0.1936	32.527